JACS
JOURNAL OF THE AMERICAN CHEMICAL SOCIETY

ARTICLE

pubs.acs.org/JACS

Atomistic Molecular Dynamics Simulations of Peptide Amphiphile Self-Assembly into Cylindrical Nanofibers

One-Sun Lee,[†] Samuel I. Stupp,[†,‡,§] and George C. Schatz*[,†,∥]

[†]Department of Chemistry, Northwestern University, 2145 Sheridan Road, Evanston, Illinois 60208-3113, United States
[‡]Department of Materials Science and Engineering, Northwestern University, Evanston, Illinois 60208-3108, United States
[§]Institute for BioNanotechnology in Medicine, Northwestern University, Chicago, Illinois 60611-2875, United States
[∥]Department of Chemical and Biological Engineering, Northwestern University, Evanston, Illinois 60208-3120, United States

ABSTRACT:

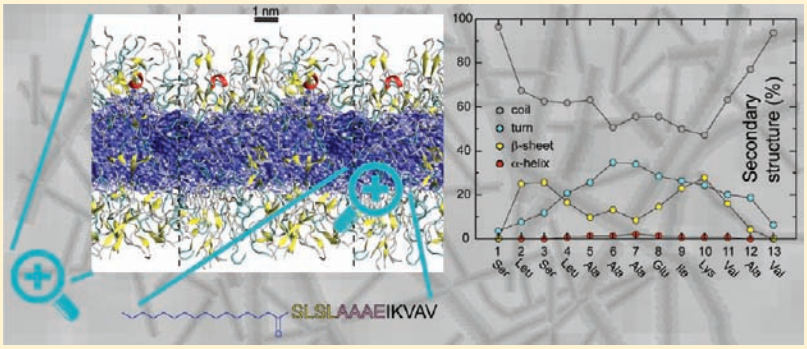

Relaxation of a self-assembled structure of 144 peptide amphiphile (PA) molecules into cylindrical nanofibers is studied using atomistic molecular dynamics simulations including explicit water with physiological ion concentration. The PA for these studies includes a hydrophobic alkyl chain that is attached to the N-terminus of the sequence SLSLAAAEIKVAV. The self-assembly is initiated with PA molecules in a roughly cylindrical configuration, as suggested from previous experimental and theoretical investigations, and the cylindrical configuration that results is found to be stable during 40 ns simulations. In the converged structure of the resulting nanofiber, the cylinder radius is ∼44 Å, a result that is consistent with experimental results. Water and sodium ions can penetrate into the peptide portion of the fiber but not between the alkyl chains. Even though each PA has an identical sequence, a broad distribution of secondary structure is found in the converged structure of the nanofiber. The β-sheet population for the SLSL and IKV segments of the peptide is ∼25%, which is consistent with previous circular dichroism results. We also found that the epitope sequence IKVAV is located on the surface of the nanofiber, as designed for the promotion of the neurite growth. Our findings will be useful for designing new PA fibers that have improved bioactive properties.

1. INTRODUCTION

There has been great interest in the self-assembly of peptide amphiphiles (PAs) into functional supramolecular structures.[1−6] In particular, Stupp and co-workers reported the self-assembly of PAs in aqueous media into cylindrical nanoscale fibers[5−7] that can be used to promote growth of blood vessels as post-infarct therapies and healing of critical wounds, bone and cartilage regeneration, axon regeneration in spinal cord injury, and other functions. They reported a class of PAs consisting of a hydrophobic segment attached to the N- or C-terminus of a peptide, with one or more charged residues, that self-assembles into nanofibers when initiated by addition of electrolyte solutions or changes in pH (Figure 1 a). A portion of a β-sheet forming sequence is intentionally inserted into the PA, and it is believed that most of the PAs adopt β-sheet secondary structure in this region, thus driving assembly into fibers as opposed to spherical or planar structures (Figure 1 b). Another domain of the peptide is a bioactive sequence that serves as the epitope for stimulating biological activity. The cell adhesion sequence RGDS from fibronectin[8,9] and the laminim-1 sequence IKVAV that is known to promote neurite sprouting are examples of possible epitope fragments that have been used.[10] In particular, an IKVAV-bearing PA has been shown to promote regeneration of both motor and sensory fibers in a mouse model of spinal cord injury.[11,12]

Many theoretical investigations have been performed to investigate the process of self-assembly and the structure of PAs-derived fibers. In particular, Schatz, Ratner, and colleagues used theories that range from simple bead and packing models to restricted atomistic calculations of clusters of PA molecules to study self-assembly.[13−18] In a study of the packing of cone-shaped objects that roughly represent the PAs, Tsonchev et al.[16] found that electrostatic interactions associated with charged residues on the peptides, along with the size difference between

Received: December 6, 2010
Published: February 22, 2011

dx.doi.org/10.1021/ja110966y | J. Am. Chem. Soc. 2011, 133, 3677–3683

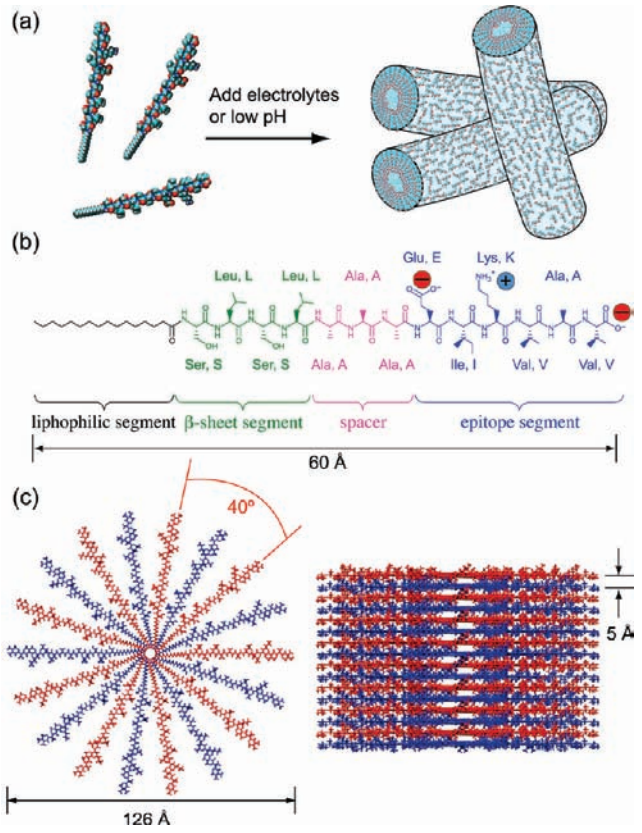

Figure 1. (a) Schematic representation of the self-assembly process of PAs. (b) PA used in MD simulation of the current report, where the PA sequence is SLSLAAAEIKVAV. (c) The starting structure of the PAs for MD simulations. Nine PAs are placed radially in the first layer (red) where their tails are pointing inward. The second layer also has 9 PAs (blue) and is rotated by 20° relative to the first layer. The angle between neighboring PAs is 40°, and the distance between layers is 5 Å.

the head and the tail of the PA, induces a void volume in the hydrophobic tail region which drives the cluster to a cylindrical rather than a spherical shape. With a finer coarse-grained model (based on the Martini model[19]), McCullagh and co-workers were able to describe the dependence of fiber formation on choice of peptide residues.[18] Also, in other work, atomistic simulations on wedge-shaped sections of the fiber using the MM2 force field revealed some aspects of the fiber structure.[16,17] However, the atomistic complexity of these calculations has prevented the generation of a converged fiber structure. A somewhat different direction was used by Olvera de la Cruz and co-workers, who developed a simplified coarse-grained model to study the influence of hydrogen-bond formation on the self-assembly of PAs.[20] They found that the interplay between hydrophobic interactions and the network of hydrogen bonds results in the formation of fiber-like assemblies in which β-sheets are parallel to the bond axis. Electrostatic interactions were not described by this model, so the relative importance of hydrogen bonds and electrostatic effects on the fiber assembly was not determined. Even with these many previous theoretical investigations, however, the atomic structure of the cylindrical nanofibers formed from PAs has not been determined, and this has proven to be a hindrance in understanding how this system functions.

In this paper, we performed a molecular dynamics (MD) simulation with the CHARMM force field of a cylindrical nanofiber composed of 144 PAs in water with physiological ion concentration (The effect of the fiber on ion concentration is negligible). The calculations show that a stable fiber structure can be generated in 40 ns simulations, which makes it possible to quantitatively examine the fiber structure and compare with experiment. We find that the most significant interaction that stabilizes the nanofiber is the electrostatic interaction between the PAs and the sodium counterions and the van der Waals interaction between the PAs. The alkyl tails usually adopt an extended random coil conformation. It is found that water and ions can penetrate the nanofiber except in the core region. Even though each PA has an identical amino acid sequence, each PA has a unique secondary structure including α-helix, β-sheet, turn, and/or coil. This enables us to quantify the fiber secondary structure, providing a detailed interpretation of a variety of structural measurements. Most of the epitope fragments are found to be exposed at the surface of the fiber, in accord with their intended design to promote neurite growth. To the best of our knowledge, this is the first simulation that has determined the structural features of cylindrical nanofibers composed of PAs at the atomistic level.

2. COMPUTATIONAL DETAILS

The peptide sequence in each PA is Ser-Leu-Ser-Leu-Ala-Ala-Ala-Glu-Ile-Lys-Val-Ala-Val; see Figure 1 b for a detailed structure. The starting structure of the backbone of each PA is assumed to be an extended conformation. To define an initial fiber structure, nine PAs are radially placed on a plane (red PAs in Figure 1 c) with the tails pointing inward. The angle between adjacent PAs is 40°. The second layer (blue PAs in Figure 1 c) is taken to be identical to the first layer but rotated by 20° relative to the first layer and with the distance between layers taken to be 5 Å. A total of 16 layers that alternate between the first and the second layers are placed along the fiber axis to define the complete structure. The starting structure was chosen based on pilot simulations we did in which fewer and greater than 9 molecules per layer were considered for the chosen diameter structure. These simulations showed that 9 molecules per layer is the highest density that leads to a stable simulation. Higher density per layer results in significant overlap between neighboring peptide amphiphiles, and the system is unstable even at the beginning of the simulations. Larger diameter structures were not considered as the diameter we chose leads to a fiber diameter that is in good agreement with experiment (see later). One hundred forty four PA molecules ($16 \times 9 = 144$) were solvated in a water box using the SOLVATE[21] module implemented in VMD.[22]

Periodic boundary conditions were used in the simulations, using a box of dimensions of $144 \times 144 \times 84$ Å^3. This box was filled with 29 953 water molecules based on the modified TIP3P potential.[23,24] To neutralize the system, 144 Na^+ ions are added. In addition to these sodium ions, another 18 Na^+ and Cl^- ions are added to make the concentration of Na^+ ion be 0.15 M. A 1000 step energy minimization was applied to the solvated system to remove the high-energy contacts.

Molecular dynamics simulations were carried out using NAMD2.[25] A 2 ns molecular dynamics simulation at 310 K with a NPT ensemble was performed to equilibrate the system. In the production period, the system was simulated for 40 ns using the NPT ensemble and Langevin dynamics[26] at a temperature of 310 K with a damping coefficient $\gamma = 5$ ps^{-1}. Pressure was maintained at 1 atm using the Langevin piston method with a piston period of 100 fs, a damping time constant of 50 fs, and a piston temperature of 310 K.[26,27] No atomic coordinates were constrained during the production period. Full electrostatics was employed using the particle-mesh Ewald method with a 1 Å grid width.[28] Nonbonded interactions were calculated using a group-based

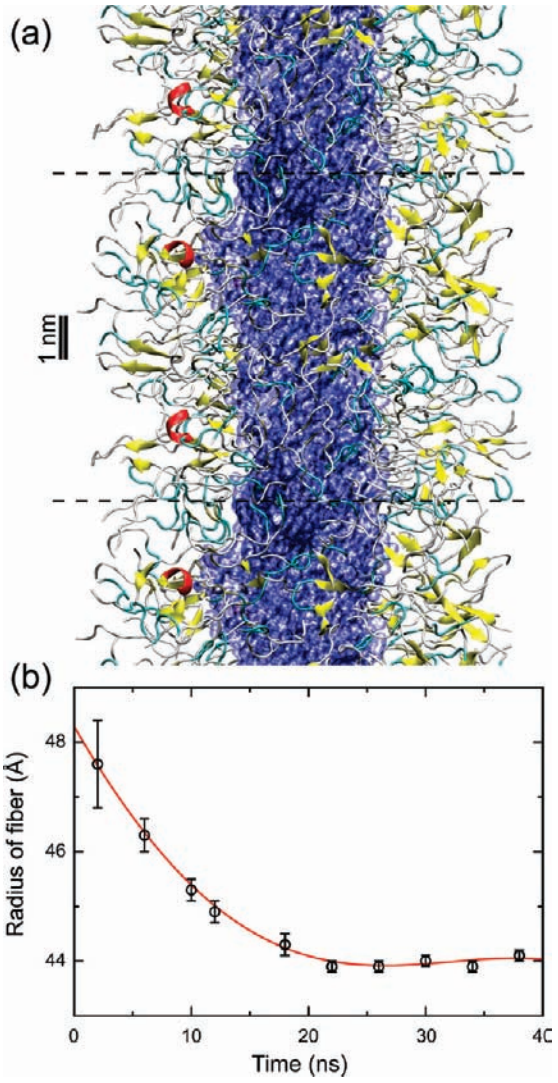

Figure 2. (a) Snapshot of self-assembled PAs at 40 ns. The hydrophobic core is represented by a blue surface: α-helixes are in red, β-sheets are in yellow, turns are in cyan, and coils are in gray. Periodic boundaries along the axis of the fiber are shown in dotted lines. (b) Radius of the fiber as a function of simulation time.

cutoff with a switching function and updated every 10 time steps. Covalent bonds involving hydrogen were held rigid using the SHAKE algorithm,[29] allowing a 2 fs time step. Atomic coordinates were saved every 10 ps for the trajectory analysis.

3. RESULTS AND DISCUSSION

A snapshot of the self-assembled PA fiber after 40 ns of simulation is shown in Figure 2 a. Periodicity along the axis of the fiber is well maintained during the simulation. In particular, PAs near the end of the primary cell have interactions with nearby PAs in neighboring image cells that are similar to the interactions between PAs in the primary cell. The density of the fiber is 19.2 PA/nm along the fiber axis. The length of the simulation cell along the axis of the fiber (z) does not change significantly during the NPT simulation, whereas the lengths of other axes (x and y) perpendicular to the z axis show a significant decrease. The fiber radius stabilizes at ~44 Å after 20 ns with only small fluctuations through 40 ns (Figure 2 b). This value is

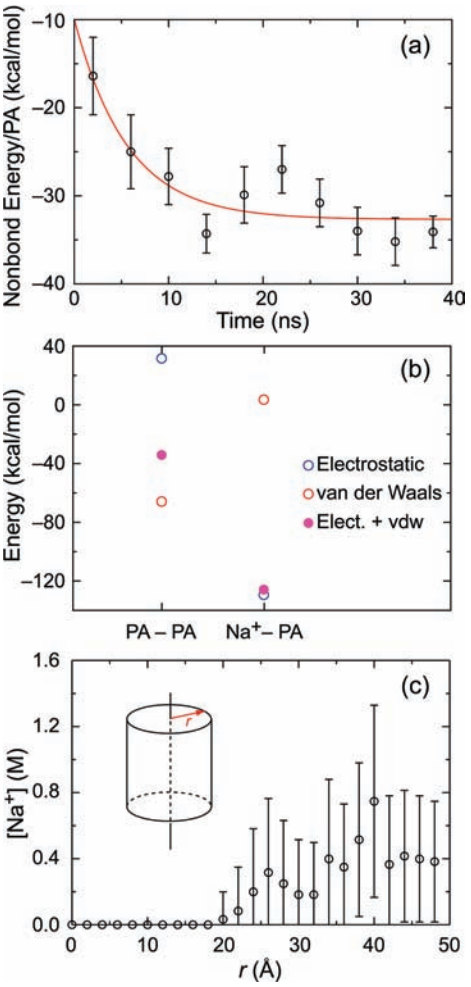

Figure 3. (a) Interaction energy of PAs as a function of simulation time. (b) Intermolecular interaction energies between PAs are shown in the left column, and interaction energies between sodium ion and PA are shown in the right column. The sum of electrostatic (open blue circle) and van der Waals energies (open red circle) is shown as a filled purple circle. (c) Distribution of sodium ions as a function of the distance from the fiber axis.

consistent with the radius of 40−50 Å obtained by vitreous ice cryo-transmission electron microscopy (TEM) experiments for cylindrical PAs consisting of 7−11 amino acids.[30] With cryo-TEM, the morphology of the PAs in aqueous solution is preserved, which means that the fiber structures should be comparable with our simulation performed in water.

The nonbonded energy (electrostatic and van der Waals) between PAs has been calculated during the simulations, and the results are presented in Figure 3 a. The contribution of the electrostatic and van der Waals energy during the last 4 ns of simulation is shown in Figure 3 b. The electrostatic energy is repulsive because each PA has a negative charge at neutral pH, whereas the van der Waals energy is attractive. The electrostatic and van der Waals energies between PAs and sodium ions is also shown in Figure 3 b. The electrostatic energy between PA and sodium ion is attractive, whereas the van der Waals energy is negligible. Therefore, the most significant interaction energies are the van der Waals interaction between PAs and the electrostatic interaction between PAs and sodium ions. In addition to these enthalpic contributions, entropic effects would provide a

significant driving force for self-assembly. Hydrogen bonding is not explicitly implemented in the CHARMM force field,[31,32] so the contribution of β-sheet formation to fiber stability cannot be directly extracted from this analysis; however, below we will explore other ways to determine hydrogen-bonding effects.

The energy analysis in our simulation is consistent with the experiments. Stendahl et al. studied the intermolecular forces associated with cylindrical PA fibers using oscillatory rheology, Fourier transform infrared spectroscopy, and circular dichroism (CD) spectroscopy.[33] They found that the self-assembly of PAs into gel-forming networks of cylindrical aggregates is triggered by counterion screening, and the cylindrical fibers are stabilized by van der Waals and hydrophobic forces, ionic bridging, and coordination and hydrogen bonding. In our simulation, we also found that the electrostatic energy between PAs and sodium ions gives the most significant contribution to the formation of cylindrical fibers.

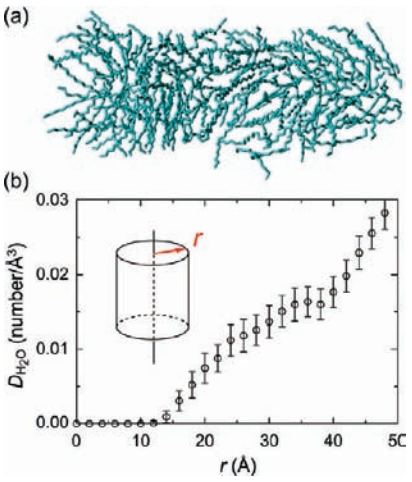

Figure 4. (a) Snapshot of the conformation of the alkyl tail of a PA fiber at 40 ns. (b) Normalized distribution of water inside the self-assembled fiber. Schematic representation of the radius of the cylindrical shape of self-assembled PA is shown in the inset of b.

The distribution of sodium ions inside the cylindrical fiber is shown in Figure 3 c. Sodium ions can penetrate to ~20 Å away from the axis of the fiber, and the concentration of sodium ions is high at $r \approx 26$ and 40 Å because the residues with negative charge (Glu and C-terminal) are located there. We also found that the van der Waals interaction between alkyl tails stabilizes the structure. About 31% of the van der Waals energy between PAs is from the interaction of alkyl tails.

A snapshot of the conformation of the alkyl tails at 40 ns is shown in Figure 4 a. Penetration of water molecules into the alkyl tails is not observed during the simulation. The distribution of water molecules inside the fiber is shown in Figure 4 b. It shows that the interior of the peptide portion of the fiber is well solvated and water molecules penetrate to around 14 Å away from the axis of the fiber. This compares well with the conclusions of Tovar et al., who used spectroscopic examination[34] to infer that the peptide region is well solvated. They also examined the alkane interior of the fibers with a hydrophobic probe, and they demonstrated that the self-assembled cylindrical PAs can be used as vehicles to sequester hydrophobic molecules such as drugs, proteins, and small organic molecules within the hydrophobic interior of the PAs.

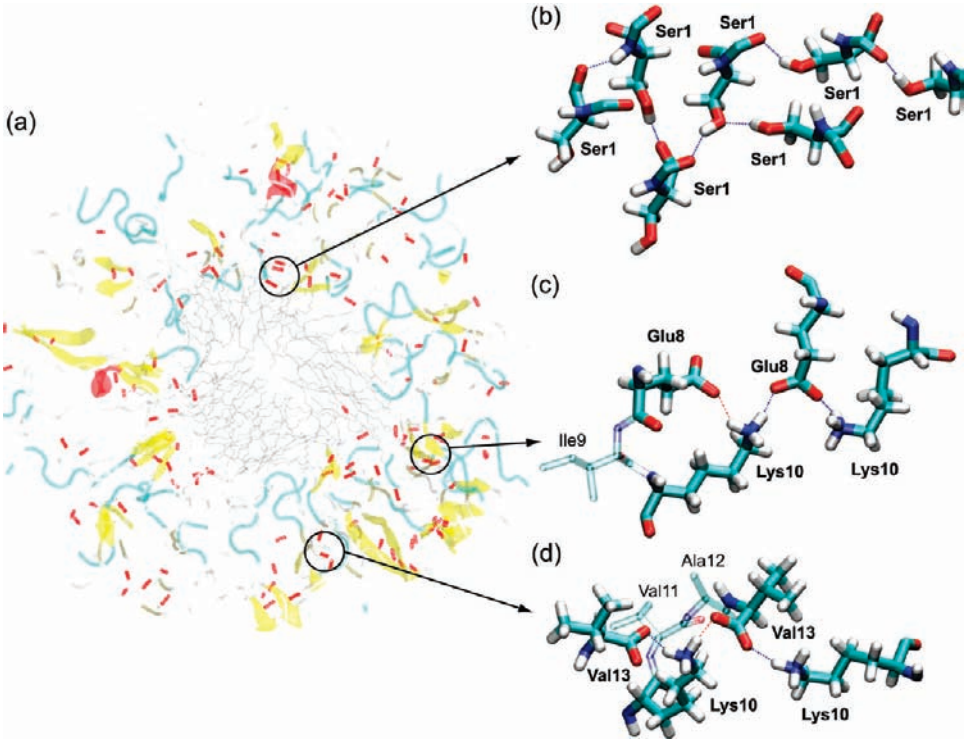

Figure 5. (a) Snapshot of the cross-section of the fiber at a simulation time of 40 ns. Hydrogen bonds are shown as red lines, whereas PAs are shown as a transparent. (b) Hydrogen bonds between serines. Salt bridges are formed between (c) lysines and glutamic acids or (d) lysines and valines. Intramolecular hydrogen bonds are shown as red dotted lines, and intermolecular hydrogen bonds are shown as blue dotted lines. Residues that are not directly involved in hydrogen bonds are shown as transparent.

Table 1. Fraction of Total Hydrogen Bonds Formed (in %)[a]

	S	L	S	L	A	A	A	E	I	K	V	A	V
S	**13.4**	**1.9**	**1.5**	0.1	0.1	0.0	0.0	0.2	0.2	0.0	0.0	0.0	0.0
L	**4.0**	0.1	0.3	0.4	0.1	0.0	0.0	0.0	0.0	0.0	0.0	0.0	0.0
S	**2.2**	**5.4**	**2.9**	**1.7**	0.6	0.1	0.0	0.6	0.0	0.2	0.1	0.0	0.0
L	0.2	0.6	**2.6**	0.8	0.1	0.0	0.0	0.0	0.0	0.0	0.0	0.0	0.0
A	0.0	0.2	0.1	**1.4**	0.4	0.1	0.1	0.1	0.0	0.0	0.0	0.0	0.0
A	0.0	0.0	0.2	0.5	**1.0**	0.2	0.1	0.4	0.0	0.0	0.0	0.0	0.0
A	0.2	0.0	0.5	0.2	**1.0**	**1.0**	**1.0**	0.7	0.0	0.0	0.1	0.0	0.0
E	0.0	0.0	0.0	0.0	0.0	0.1	0.7	0.3	0.2	0.0	0.1	0.0	0.0
I	0.0	0.0	0.0	0.0	0.0	0.1	0.2	**2.1**	0.0	**1.6**	0.0	0.3	0.0
K	0.0	0.2	0.2	0.2	0.2	0.1	**1.4**	**22.5**[b]	**3.3**	**1.3**	0.9	0.5	**6.4**[b]
V	0.0	0.0	0.0	0.0	0.1	0.0	0.0	0.2	0.0	**1.7**	0.3	0.1	0.0
A	0.0	0.0	0.0	0.0	0.0	0.0	0.2	0.4	**1.0**	0.5	**1.8**	0.0	0.2
V	0.0	0.0	0.0	0.0	0.0	0.0	0.0	0.1	0.0	0.1	0.0	0.0	0.0

[a] The population of hydrogen bonds is calculated based on the number of hydrogen bonds summed over all donor−acceptor pairs. The criteria for formation of hydrogen bonds are (1) H−A < 3.0 Å and (2) D−H−A > 160°, where D is donor, A is acceptor, and H is hydrogen. Amino acids in italics are donors, and amino acids in roman are acceptors for hydrogen bonding. Percentage more than 1% is written in bold. [b] Salt bridges.

During the simulation we found that there are a lot of hydrogen-bonding interactions between PAs, as suggested in the experimental work. A snapshot of the hydrogen-bonding network that is generated by the PAs is shown in Figure 5 a. An analysis of intermolecular hydrogen bonding during the last 4 ns of the simulation is shown in Table 1. Each residue of each PA can act as a donor or acceptor. (Donors are in italic font and acceptors in roman font in Table 1) and only intermolecular hydrogen bonds (i.e., between PAs) are shown. The population of hydrogen bonds is calculated based on the number of intermolecular hydrogen bonds found summed over donor−acceptor pairs for each PA, averaged over the last 4 ns of the MD simulation. Most of the hydrogen bonds are found along the diagonal part of Table 1, so since the PA's point radially, the intermolecular hydrogen bonds are perpendicular to the radial coordinate. (Below we show that they are predominantly parallel to the fiber axis.) About 38% of the hydrogen bonding occurs at residues 1−4 (Ser-Leu-Ser-Leu). A snapshot of the hydrogen bonding between serines is shown in Figure 5 b. Both the side chain and the backbone are involved in hydrogen bonding. We also find that salt bridges are formed between Lys and Glu and between Lys and Val (C-terminal). Hydrogen bonding occurs both intra- and intermolecularly between PAs as shown in Figure 5 c and 5d. This is consistent with the experiments reported by Paramonov et al.[35] They examined the role of hydrogen bonding in the self-assembled cylindrical PAs by varying the peptide sequence, and they found that hydrogen bonding close to the hydrophobic core was necessary to form cylindrical nanofibers from PAs.

Even though the starting structure of each PA is an extended conformation (Figure 1) and the sequence of each PA is identical, we found a broad distribution of secondary structures in the peptides after 40 ns MD simulation. The distribution of secondary structure along the sequence of the PAs is shown in Figure 6 a (based on the calculations using the stride[36,37]), and the average population of the secondary structure of the PAs is shown in Table 2. Figure 6 a shows that the β-sheet population is

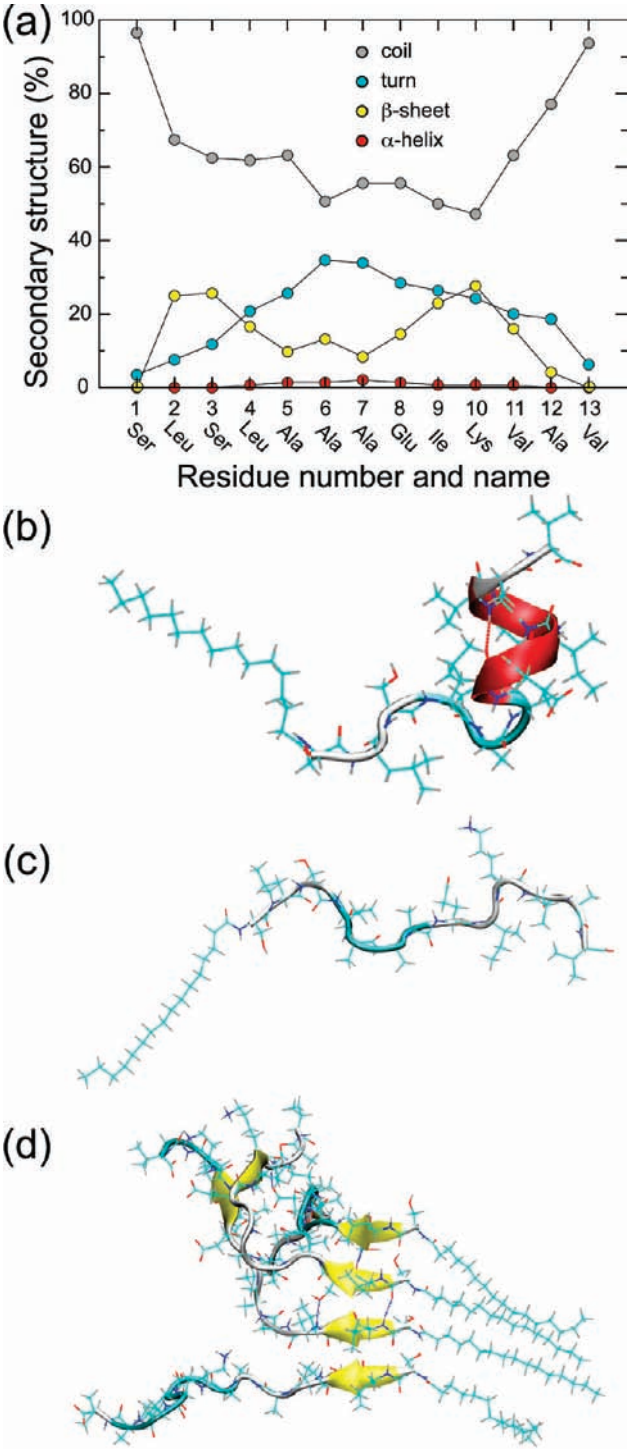

Figure 6. (a) Distribution of secondary structure of the PAs along the peptide sequence. α-Helixes are usually formed in the middle of the PA, while β-sheets are formed in residues 2−4 and 9−11. Representative PA conformations in the fiber, including (b) α-helixes, (c) coils and turns, and (d) β-sheets in the self-assembled fiber. The direction of the β-sheets is predominantly parallel to the axis of fiber.

higher (~25%) at residues 2−4 and 9−11, whereas the average β-sheet population is ~14%. This is consistent with previous experiments reported by Niece et al.[38] They quantified the secondary structure of IKVAV-bearing PAs using CD spectra, and they found that the β-sheet population is ~25 ± 20%. The

dx.doi.org/10.1021/ja110966y | J. Am. Chem. Soc. 2011, 133, 3677–3683

Table 2. Average Population of the Secondary Structure of PAs in Fiber

configuration	percentage (%)
α-helix	1
β-sheet	14
turn	20
coil	65

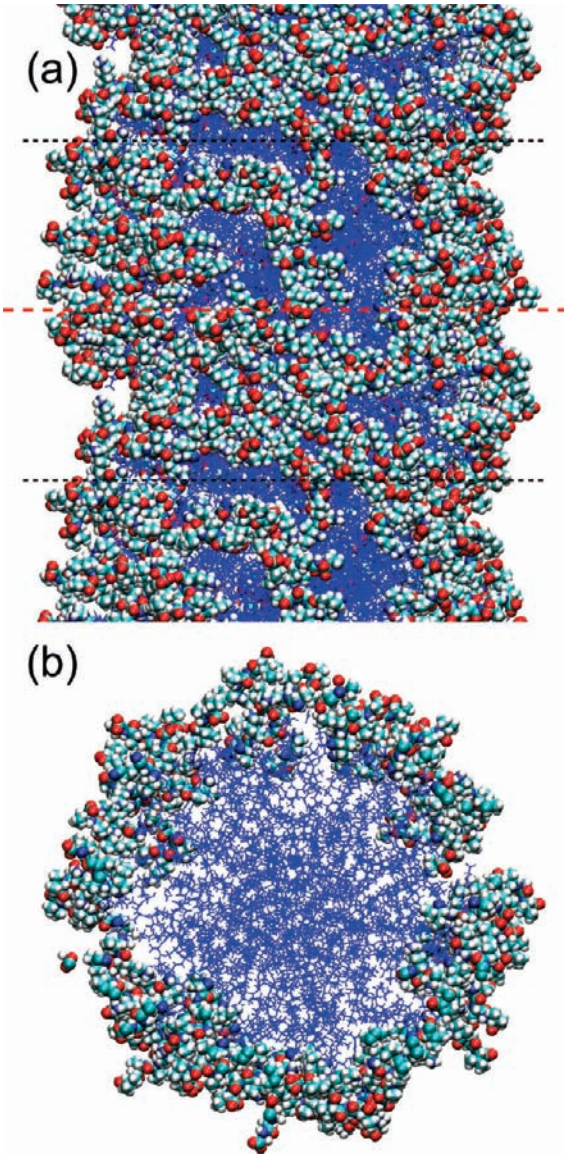

Figure 7. (a) Snapshot (at 40 ns) of the side view of the fiber, showing the epitope (IKVAV) segment. Atoms in the epitopes are shown as solid spheres, whereas other parts of the PAs are shown as blue lines. Periodic boundaries along the axis of the fiber are shown as black dotted lines. (b) Top view of the cross section of the fiber along the red dotted line shown in a.

α-helix population in their experiments was estimated as ∼45 ± 35% in their analysis, whereas it is only ∼1% in our simulation (Figure 6 a and 6b). However, the α-helix population of IKVAV-bearing PAs shows a broad range in the experiments, from less than 10% to ∼80%.[38] In our simulation, the dominant secondary structure is the random coil over the entire sequence (Figure 6 a and 6c). Behanna et al. found that PAs with positive or negative net charge have a tendency to adopt a random coil secondary structure.[7] Jiang et al. also found that the conformation of a PA containing the IKVAV epitope is statistically more disorganized based on polarization modulation-infrared reflection−absorption spectroscopy.[39] In our simulation, the direction of the β-sheets is predominantly parallel with the fiber axis (Figure 6 d). This is consistent with earlier theoretical studies[20] and provides a mechanism for the formation of cylindrical fibers rather than spherical structures. The β-sheets found in our simulation, however, are scattered around the inside of nanofiber and do not show the continuous β-sheet structure along the fiber axis that was previously suggested using simple models.[20] It has been suggested that the formation of β-sheets parallel to the axis of the fiber is the driving force for the formation of cylindrical fibers rather than spherical micelles.[20,30,33,39] This model, however, does not require that the β-sheets are infinitely continuous along the fiber. According to Niece et al.,[38] the fraction of β-sheet in the PAs varies from ∼5 to ∼45% depending on the amino acid sequence, yet even with this variation, the PAs self-assemble into fibers. Our simulations show 14% β-sheets and that the sheets are predominantly parallel to the fiber axis. Therefore, our simulation result is consistent with the previous model of β-sheets parallel to the fiber axis driving fiber formation.

The conformation of the epitope segment is another issue of interest concerning the IKVAV-containing PAs because it is known that IKVAV promotes neurite growth.[10] Indeed, Jiang et al. reported that the conformational freedom of IKVAV helps the effective expression of the IKVAV epitope on the surface of the PA fibers. As shown in Figure 7a and 7b, most of IKVAV epitopes are located on the surface of the fiber in our simulation.

4. CONCLUSION

In summary, we performed 40 ns MD simulations for a cylindrical nanofiber composed of 144 PAs in water with 0.15 M sodium ion concentration at a fully atomistic level. During the simulation, the periodicity is well maintained along the axis of the fiber, and the radius of the fiber is ∼44 Å, a result that compares sensibly with experimental results. Through an analysis of the nonbonded interaction energy, we found that the energy that stabilizes the cylindrical fiber is the electrostatic energy between the PAs and the sodium ions as well as the van der Waals energy between the PAs. No water is found in the region of the alkyl tail, but water molecules can penetrate as close as ∼14 Å from the fiber axis. The hydrogen-bonding network is most significant in the SLSL region, while salt bridges are formed between the charged residues. We also found that the β-sheet secondary structure has a higher population (25%) in the SLSL region and the amount of hydrogen bonding is similar to that inferred in the experiments. β-Sheets are mostly along the fiber axis, which provides a driving force for making cylindrical fibers. In addition, the epitope region of the PA that is designed for the promotion of neurite outgrowth is exposed at the surface of the fiber. The atomistic structure of PA fibers reported in this work will be useful for designing new PAs and PA fibers that have potentially improved biological activities and functions.

■ AUTHOR INFORMATION

Corresponding Author
schatz@chem.northwestern.edu

■ ACKNOWLEDGMENT

This research was supported by the National Science Foundation (grant CHE-0843832), by the NSEC Center at Northwestern (NSF grant EEC-0647560), and by the DOE NERC EFRC (DE-SC0000989).

■ REFERENCES

(1) Murakami, Y.; Nakano, A.; Fukuya, K. *J. Am. Chem. Soc.* **1980**, *102*, 4253.
(2) Murakami, Y.; Nakano, A.; Yoshimatsu, A.; Uchitomi, K.; Matsuda, Y. *J. Am. Chem. Soc.* **1984**, *106*, 3613.
(3) Vauthey, S.; Santoso, S.; Gong, H. Y.; Watson, N.; Zhang, S. G. *Proc. Natl. Acad. Sci. U.S.A.* **2002**, *99*, 5355.
(4) Shimizu, T.; Masuda, M.; Minamikawa, H. *Chem. Rev.* **2005**, *105*, 1401.
(5) Hartgerink, J. D.; Beniash, E.; Stupp, S. I. *Science* **2001**, *294*, 1684.
(6) Hartgerink, J. D.; Beniash, E.; Stupp, S. I. *Proc. Natl. Acad. Sci. U.S.A.* **2002**, *99*, 5133.
(7) Behanna, H. A.; Donners, J.; Gordon, A. C.; Stupp, S. I. *J. Am. Chem. Soc.* **2005**, *127*, 1193.
(8) Pierschbacher, M. D.; Ruoslahti, E. *Nature* **1984**, *309*, 30.
(9) Storrie, H.; Guler, M. O.; Abu-Amara, S. N.; Volberg, T.; Rao, M.; Geiger, B.; Stupp, S. I. *Biomaterials* **2007**, *28*, 4608.
(10) Silva, G. A.; Czeisler, C.; Niece, K. L.; Beniash, E.; Harrington, D. A.; Kessler, J. A.; Stupp, S. I. *Science* **2004**, *303*, 1352.
(11) Tysseling-Mattiace, V. M.; Sahni, V.; Niece, K. L.; Birch, D.; Czeisler, C.; Fehlings, M. G.; Stupp, S. I.; Kessler, J. A. *J. Neurosci.* **2008**, *28*, 3814.
(12) Tysseling, V. M.; Sahni, V.; Pashuck, E. T.; Birch, D.; Hebert, A.; Czeisler, C.; Stupp, S. I.; Kessler, J. A. *J. Neurosci. Res.* **2010**, *88*, 3161.
(13) Tsonchev, S.; Niece, K. L.; Schatz, G. C.; Ratner, M. A.; Stupp, S. I. *J. Phys. Chem. B* **2008**, *112*, 441.
(14) Tsonchev, S.; Schatz, G. C.; Ratner, M. A. *Nano Lett.* **2003**, *3*, 623.
(15) Tsonchev, S.; Schatz, G. C.; Ratner, M. A. *J. Phys. Chem. B* **2004**, *108*, 8817.
(16) Tsonchev, S.; Troisi, A.; Schatz, G. C.; Ratner, M. A. *J. Phys. Chem. B* **2004**, *108*, 15278.
(17) Tsonchev, S.; Troisi, A.; Schatz, G. C.; Ratner, M. A. *Nano Lett.* **2004**, *4*, 427.
(18) McCullagh, M.; Prytkova, T.; Tonzani, S.; Winter, N. D.; Schatz, G. C. *J. Phys. Chem. B* **2008**, *112*, 10388.
(19) Marrink, S. J.; Risselada, H. J.; Yefimov, S.; Tieleman, D. P.; de Vries, A. H. *J. Phys. Chem. B* **2007**, *111*, 7812.
(20) Velichko, Y. S.; Stupp, S. I.; de la Cruz, M. O. *J. Phys. Chem. B* **2008**, *112*, 2326.
(21) Grubmuller, H. *SOLVATE*, 1.2 ed.; Theoretical Biophysics Group, Institute for Medical Optics, Ludwig-Maximilian University: Munich, 1996.
(22) Humphrey, W.; Dalke, A.; Schulten, K. *J. Mol. Graph.* **1996**, *14*, 33.
(23) Jorgensen, W. L.; Chandrasekhar, J.; Madura, J. D.; Impey, R. W.; Klein, M. L. *J. Chem. Phys.* **1983**, *79*, 926.
(24) Mackerell, A. D.; Wiorkewiczkuczera, J.; Karplus, M. *J. Am. Chem. Soc.* **1995**, *117*, 11946.
(25) Kale, L.; Skeel, R.; Bhandarkar, M.; Brunner, R.; Gursoy, A.; Krawetz, N.; Phillips, J.; Shinozaki, A.; Varadarajan, K.; Schulten, K. *J. Comput. Phys.* **1999**, *151*, 283.
(26) Martyna, G. J.; Tobias, D. J.; Klein, M. L. *J. Chem. Phys.* **1994**, *101*, 4177.
(27) Feller, S. E.; Zhang, Y. H.; Pastor, R. W.; Brooks, B. R. *J. Chem. Phys.* **1995**, *103*, 4613.
(28) Darden, T.; York, D.; Pedersen, L. *J. Chem. Phys.* **1993**, *98*, 10089.
(29) Andersen, H. C. *J. Comput. Phys.* **1983**, *52*, 24.
(30) Pashuck, E. T.; Cui, H. G.; Stupp, S. I. *J. Am. Chem. Soc.* **2010**, *132*, 6041.
(31) Ferguson, D. M.; Kollman, P. A. *J. Comput. Chem.* **1991**, *12*, 620.
(32) MacKerell, A. D.; Bashford, D.; Bellott, M.; Dunbrack, R. L.; Evanseck, J. D.; Field, M. J.; Fischer, S.; Gao, J.; Guo, H.; Ha, S.; Joseph-McCarthy, D.; Kuchnir, L.; Kuczera, K.; Lau, F. T. K.; Mattos, C.; Michnick, S.; Ngo, T.; Nguyen, D. T.; Prodhom, B.; Reiher, W. E.; Roux, B.; Schlenkrich, M.; Smith, J. C.; Stote, R.; Straub, J.; Watanabe, M.; Wiorkiewicz-Kuczera, J.; Yin, D.; Karplus, M. *J. Phys. Chem. B* **1998**, *102*, 3586.
(33) Stendahl, J. C.; Rao, M. S.; Guler, M. O.; Stupp, S. I. *Adv. Funct. Mater.* **2006**, *16*, 499.
(34) Tovar, J. D.; Claussen, R. C.; Stupp, S. I. *J. Am. Chem. Soc.* **2005**, *127*, 7337.
(35) Paramonov, S. E.; Jun, H. W.; Hartgerink, J. D. *J. Am. Chem. Soc.* **2006**, *128*, 7291.
(36) Frishman, D.; Argos, P. *Proteins* **1995**, *23*, 566.
(37) Heinig, M.; Frishman, D. *Nucleic Acids Res.* **2004**, *32*, W500.
(38) Niece, K. L.; Czeisler, C.; Sahni, V.; Tysseling-Mattiace, V.; Pashuck, E. T.; Kessler, J. A.; Stupp, S. I. *Biomaterials* **2008**, *29*, 4501.
(39) Jiang, H. Z.; Guler, M. O.; Stupp, S. I. *Soft Matter* **2007**, *3*, 454.